

# Shaping of the inner Oort cloud by Planet Nine

Erez Michaely and <sup>1</sup>★, Abraham Loeb<sup>2</sup>

<sup>1</sup>*Physics Department, Technion - Israel Institute of Technology, Haifa 3200004, Israel*

<sup>2</sup>*Department of Astronomy, Harvard University, 60 Garden St., Cambridge, MA 02138, USA*

Accepted XXX. Received YYY; in original form ZZZ

## ABSTRACT

We present a numerical simulation of the dynamical interaction between the proposed Planet Nine and a debris disk around the Sun for 4Gyr, accounting for the secular perturbation of the four giant planets in two scenarios: (a) an initially thin circular disk around the Sun (b) inclined and eccentric disk. We show, in both scenarios, that Planet Nine governs the dynamics in between 1000–5000AU and forms spherical structure in the inner part ( $\sim 1000$  AU) and inclined disk. This structure is the outcome of mean motion resonances and secular interaction with Planet Nine. We compare the morphology of this structure with the outcome from a fly-by encounter of a star with the debris disk and show distinct differences between the two cases. We predict that this structure serves as a source of comets and calculate the resulting comet production rate to be detectable.

**Key words:** Kuiper belt: general– Oort Cloud – planets and satellites: dynamical evolution and stability

## 1 INTRODUCTION

The structure of the outer solar system is complex and interesting. Oort (1950) explained the isotropic distribution of long-period comets, by conjecturing with the existence of a Sun-centred spherical cloud with inner semi-major axis (sma) of  $2 \times 10^4$  AU and an outer sma of  $2 \times 10^5$  AU. Later work by Marsden et al. (1978) extended the inner sma to  $1 \times 10^4$  AU. Oort showed that the comet reservoir can easily be perturbed by frequent distant stellar encounter and the Galactic tides. These perturbations can drive the objects in the Oort cloud to the inner-solar system with eccentricities close to unity, yielding the constant rate of Sun grazing comets.

Hills (1981) suggested that the inner boundary of the Oort cloud reflects an observational bias, and the actual inner boundary is closer than  $2 \times 10^4$  AU. He found that the critical sma  $a_c$  that satisfies both the rate of stellar encounters and a typical comet lifetime is  $a_c = 2 \times 10^4$  AU. In this model, the inner Oort cloud (“Hills cloud”) continues inward of  $2 \times 10^4$  AU but stellar encounters that on this scale occur on a longer timescale than the typical lifetime of comets. Therefore, on these scales there should be a burst of comet showers after each stellar encounter.

Duncan et al. (1987) studied numerically how the Oort and Hills clouds were formed. They focused on scattering by the planets to high sma and the interaction with the Galactic tides and stellar perturbations and found that the inner part of the Hills cloud is  $\sim 3 \times 10^3$  AU.

Recently Batygin & Brown (2016) reported intriguing evidence for the existence of a ninth planet in our solar system

(Batygin & Brown 2016; Trujillo & Sheppard 2014). The proposed Planet Nine has a mass of  $m_9 = 10m_\oplus$ , sma of  $a_9 = 700$  AU, eccentricity  $e_9 = 0.6$ , inclination to the ecliptic,  $i_9 = 30^\circ$ , and argument of the periapsis,  $\omega_9 = 130^\circ$ . Several other follow up studies supported the existence of Planet Nine by different methods (Fienga et al. 2016; Holman & Payne 2016; Bailey et al. 2016; Gomes et al. 2017; Lai 2016). Additionally, Li & Adams (2016) calculated the survival rates and the interaction cross section of the proposed planet, and Lawler et al. (2016) investigated the impact of Planet Nine of the Kuiper belt objects. Perets & Kouwenhoven (2012) described a mechanism of a planet captured from a different star system or a rouge planet, and predicted a wide, eccentric and inclined orbit of the captured planet.

In this work we explore the interaction of a captured Planet Nine with a debris disk in two scenarios: (a) an initially flat ecliptic disk around the Sun and (b) an initially inclined and eccentric disk. The disk we consider represents the early debris disk, remnant from the Sun’s formation era. For a short-term interaction of a planet with a ring of debris around it, see Lee & Chiang (2016). We show that Planet Nine, due to its large sma, dominates the evolution of the outer disk between 1000–5000AU. This results in a spheroidal structure at  $1100 \text{ AU} \lesssim a_{\text{TAUS}} \lesssim 1500 \text{ AU}$  where TAUS stands for “Thousand AU Sphere”. For scenario (a) this structure is surrounded by an inclined disk aligned with Planet Nine’s orbital plane and a warped disk towards the ecliptic plane. For scenario (b) the TAUS and inclined disk are created but less visible due to the initial conditions. This structure serves as a new source of Sun grazing comets, penetrating the inner solar system by long term secular evolution and dynamical interaction with Planet Nine.

Our paper is organized as follows: in section 2 we describe the

★ E-mail: eretzmichaely@gmail.com

numerical simulation. In section 3 we describe the results of the numerical runs in comparison to the standard Hills cloud formation mechanism, i.e. a fly-by event in the early stages of the solar system. In section 4 we present the implications of TAUS to the morphology of the outer solar system as well as the rate and orientation of comets originating from this region. Finally, we summarize the results and their implications in section 5.

## 2 NUMERICAL EXPERIMENTS

We used the code MERCURY6 (Chambers 1999), N-body code with a the Bulirsch-Stoer algorithm. The timestep used was 185 days which is one thousandth of the period of Planet Nine around the Sun ( $\sim 10^{-3}P_9$ ) and accuracy parameter of  $10^{-12}$ . Only the Sun and Planet Nine were treated explicitly while the rest of the four giant planets (Jupiter, Saturn, Uranus and Neptune) were included secularly via their  $J_2$  moment term

$$J_2 = \frac{1}{2} \sum_{i=1}^4 \frac{m_i a_i^2}{MR^2} \quad (1)$$

where  $m_i$  and  $a_i$  are the mass and its sma of planet number  $i$  respectively.  $R = a_4$  is the effective radius of the inner solar system which was set to be the orbital sma of Neptune. Any particle that crossed  $R$  (from outside) was removed from the integration. We can neglect the Galactic tides effects up to the scale of  $\sim 10^4$  AU (Veras & Evans 2013).

For scenario (a) we simulated an initially flat and circular debris disk around the Sun with 32,000 massless particles of surface density profile  $\sigma \propto a^{-\gamma}$ , with  $\gamma = -1$  and  $a$  being the massless particle sma (Andrews et al. 2010). Larwood & Kalas (2000) and Kalas et al. (2000) use a different power-law index,  $\gamma = -3/2$ ; this value has only a minor effect on the results presented in section 3. The region of the disk encompasses  $700\text{AU} < a < 7000\text{AU}$ , with eccentricity chosen from a flat distribution in the range  $e \in \{0, 0.1\}$ . The initial inclination  $i = 0$ , so that the longitude of the ascending nodes,  $\Omega$ , and the argument of the periastris,  $\omega$ , are ill defined. The mean anomaly  $\mathcal{M}$  was drawn from a flat distribution of angles in the range  $\mathcal{M} \in \{0, 360^\circ\}$ . For scenario (b) we simulated 32,000 massless particles with surface density and sma distribution as in scenario (a). We used thermal distribution for the eccentricity and inclination drawn uniformly from a distribution with aspect ratio of 0.1, for the vertical distance over the distance from the Sun. The argument of pericentre the longitude of the ascending node and the mean anomaly were drawn randomly from a flat distribution of angles between 0 and  $360^\circ$ .

Planet Nine parameters were taken from Batygin & Brown (2016) and Brown & Batygin (2016), with  $m_9 = 10m_\oplus$ ,  $a_9 = 700\text{AU}$ ,  $e_9 = 0.6$ ,  $i_9 = 30^\circ$ ,  $\omega_9 = 130^\circ$ ,  $\Omega_9 = 0$  and  $\mathcal{M} = 0$ . Since the giant planets are incorporated through  $J_2$  and the disk has cylindrical symmetry, the exact value of  $\Omega_9$  has no physical significance.

We integrated the system for 4Gyr and followed the change of the orbital parameters as well as morphology of the debris disk. The results from these simulations are presented in the next section.

## 3 RESULTS

In this section we present the numerical integration results for the two scenarios described in section 2. Subsection 3.1 is dedicated for

scenario (a) i.e. flat and circular initial disk. In subsection 3.2 we present the results for scenario (b), namely for initially inclined and eccentric disk. Both subsection present the results after integrating the system for 4Gyr, and in both we find three qualitatively different regions of the disk: (i) The most inner stable part of the disk has a *spheroidal structure* (TAUS); (ii) beyond the sphere there is an *inclined disk* with respect to the ecliptic; and (iii) beyond the inclined part of the disk, reside a disk warped back to the ecliptic plane.

### 3.1 Scenario (a)

Figure 1 presents several snapshots from the scenario (a) at an edge-on view relative to the ecliptic plane in the outer solar system at different times, with the x-direction chosen arbitrarily and the y-direction is aligned with the orbital angular momentum of the ecliptic plane. Figure 2 presents an edge-on view from Planet Nine's orbital plane. At this orientation, Planet Nine's orbital angular momentum is pointing in the y-direction and the line of nodes is perpendicular to the origin. The spheroidal structure is visible from both perspectives.

The structure of the disk is complex. Figure 3 presents the eccentricity, inclination, argument of pericentre and the longitude of the ascending node of the test particles as a function of the sma. The results exhibit a spread in inclination, eccentricity and the longitude the ascending nodes. This implies a spherical like structure up to 1500AU which decline gradually with distance. The complexity originates from mean motion resonances (MMRs) with Planet Nine and secular interaction with Planet Nine's orbit (Murray & Dermott 1999). MMRs are caused when the ratio of the orbital periods  $P_1$  and  $P_2$  is a rational number,

$$\frac{\alpha}{\beta} = \frac{P_1}{P_2} = \left(\frac{a_1}{a_2}\right)^{3/2}, \quad (2)$$

with  $\alpha$  and  $\beta$  being (small) integers. In MMRs the resonant angle  $\phi$  defined as

$$\phi = j_1 \lambda_9 + j_2 \lambda + j_3 \varpi_9 + j_4 \varpi + j_5 \Omega_9 + j_6 \Omega, \quad (3)$$

where  $\lambda$  is the mean longitude,  $\varpi$  is the longitude of pericentre and  $\Omega$  is the longitude of the ascending node. The prefactors  $j_i$  satisfies

$$\sum_i j_i = 0. \quad (4)$$

A fingerprint of MMR involves the excitation of orbital parameters at specific period ratio with the basic frequency, i.e. the mean motion frequency of Planet Nine. The vertical lines in figure 6 are the locations of main MMRs with Planet Nine. Different colour of vertical lines correspond to different order of resonance. The proximity of the resonances below 3 : 1 suggests that the dynamics in this regions are influenced by MMR overlap (Morbidelli et al. 1995). The resonances above 3 : 1 are isolat. Further evidence for the importance of the MMRs is presented in figure 5. The distinction between isolated and overlapping MMRs is clear below the 3 : 1 resonance. The analytic treatment of the MMRs goes beyond the scope of this manuscript. The inner part TAUS shows clustering in  $\omega$  and  $\Omega$ . The rest of the disk has two regions: the inclined region  $1500\text{AU} < a < 3000\text{AU}$  which is aligned with Planet Nine's orbital plane similar with (Mouillet et al. 1997) and the flat disk on the ecliptic plane.

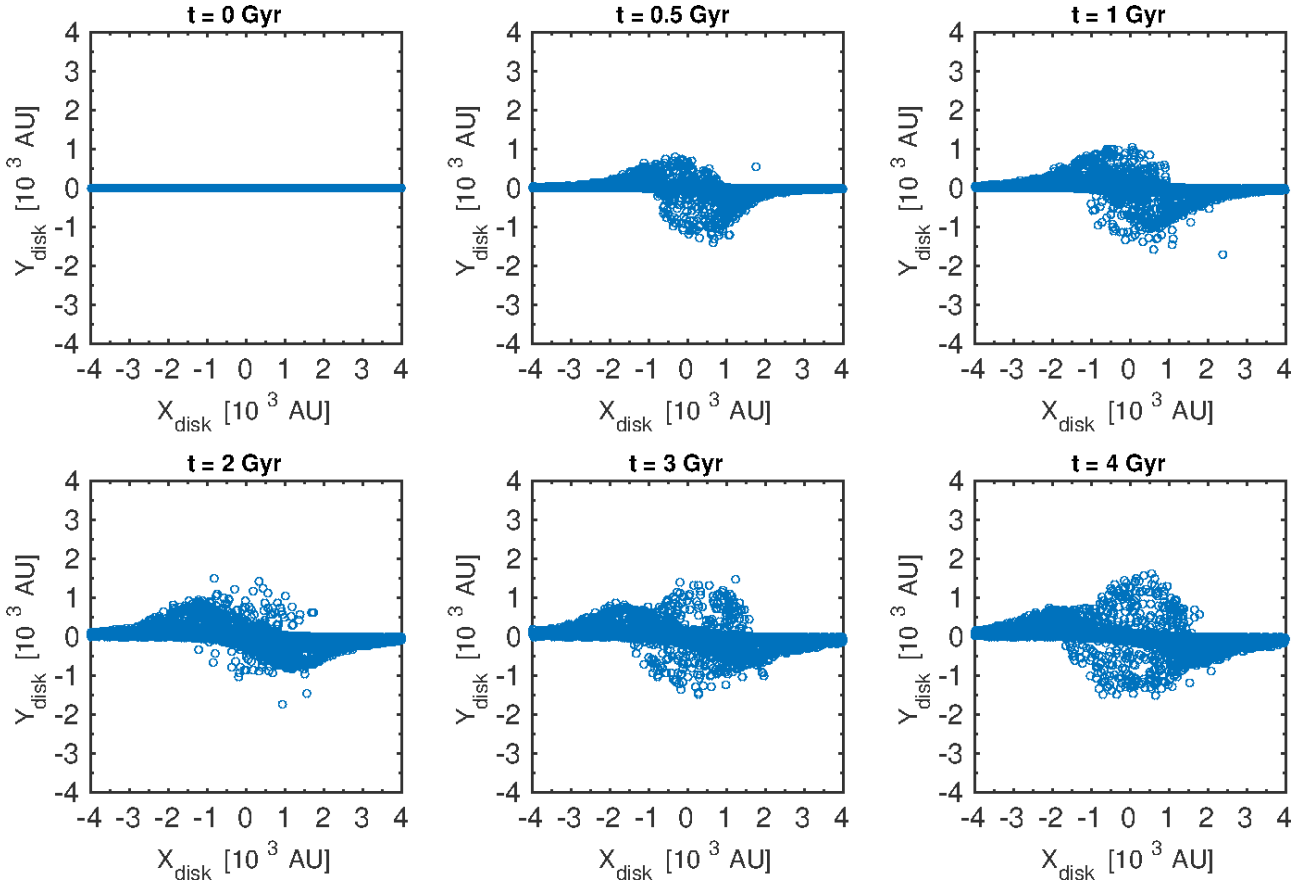


**Figure 1.** Edge on view of the outer solar system at 0.5, 1, 2, 3, 4 Gyr after formation. The centre notes the Sun and the blue circles are the massless particles. Panel (a) provides a snapshot of the initial conditions for a flat non inclined disk with inner cutoff of 700AU and an outer cutoff of 7000AU. At the final snapshot  $t = 4$ Gyr, all three regions of the disk are visible: (i) the TAUS at a radius of  $\sim 1500$ AU; (ii) an inclined disk, about  $20^\circ$  from the ecliptic plane, between  $1500\text{AU} < a < 3000\text{AU}$  and (iii) a warped disk relative to the ecliptic plane, at  $a \gtrsim 3000\text{AU}$ .

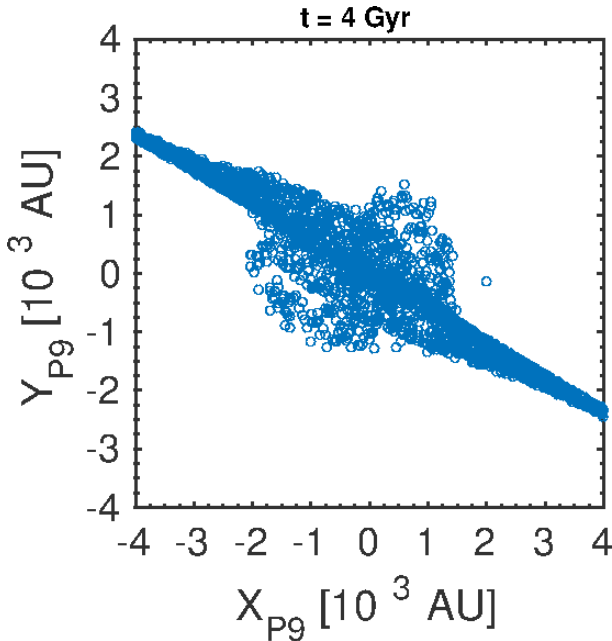


**Figure 2.** The same as Figure 1 with the y-axis aligned with Planet Nine's orbital angular momentum. The line of node is perpendicular to the displayed plane.

### 3.2 Scenario (b)

Next we present the structure of the disk in the second scenario, of an inclined and eccentric initial disk. The underlying structure of the final state is similar to scenario (a). The basic structure of spherical TAUS and inclined disk is supplemented by hot and inclined group of test particles. Figure 6 present the final orbital elements as a function of sma. Unsurprisingly the TAUS is extended toward 3000AU distance. The cold inclined disk is visible in the inclination plot. Two specific sets of test particles are presented in Fig. 8. The left panel presents the evolution of an inclined particle while the right panel shows the evolution of ejected particles. In both cases the resonant angle  $\phi$  is plotted versus time.

We also examine the final distributions in the properties of the relevant orbital elements of the different disk regions (shown in both scenarios): TAUS, inclined disk, and the warped+ecliptic disk. We consider each region separately.

### 3.3 TAUS

TAUS is the spheroidal region of the disk located between  $1000\text{AU} \lesssim a \lesssim 1500\text{AU}$ . The distribution of the eccentricities,  $e$ , the longitude of the ascending node,  $\Omega$ , and the argument of periaapsis,  $\omega$ , are presented in the appendix at A1. TAUS maintains highly eccentric orbits, with  $e > 0.8$ . Since particles with periaapsis distance of  $q \leq a_{\text{Neptune}}$  are removed from the integration, the

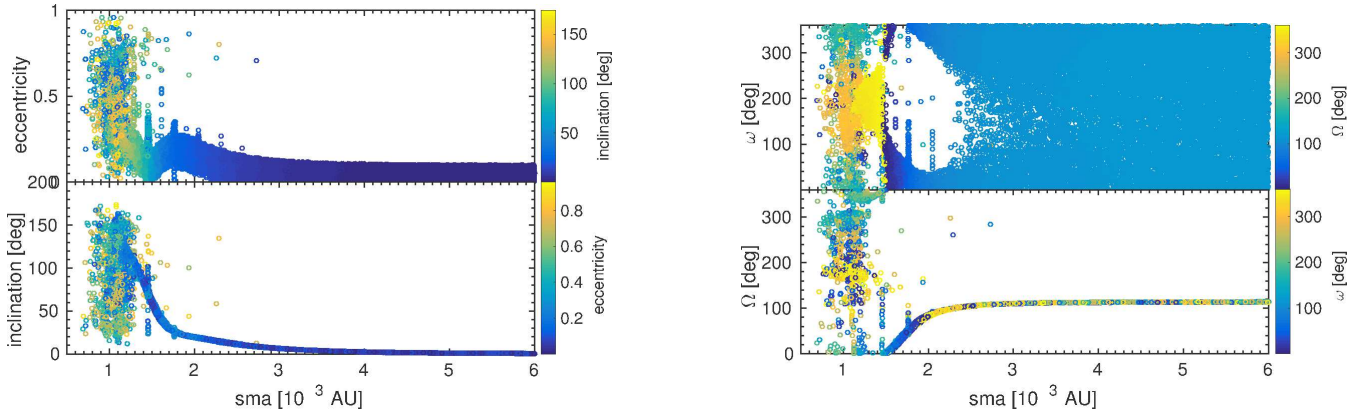


**Figure 3.** Left panel: the final inclination and eccentricity distributions as a function of sma, with eccentricity and inclination, respectively, colour coded. Right panel: the final argument of pericentre and the longitude of the ascending node final distribution as a function of sma.

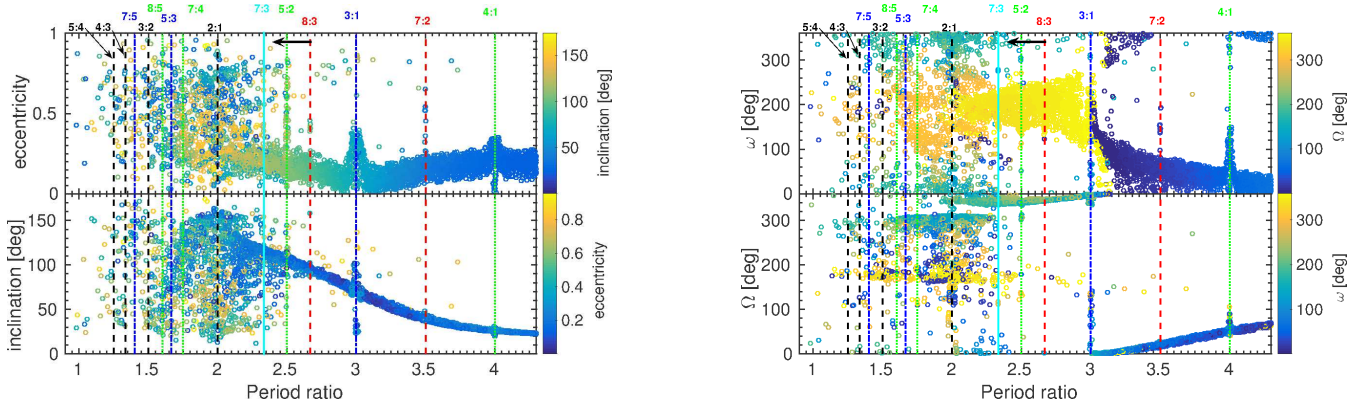


**Figure 4.** Left panel: the final state of eccentricities and inclinations as a function of period ratio. The vertical lines corresponds to the main MMRs. Order 1 black; order 2 blue; order 3 green; order 4 cyan; order 5 red. The black arrow indicate the end of the TAUS at 1500AU. Right panel: the final distribution of the argument of pericentre and the longitude of the ascending nodes. In both panel the MMRs are visible.

eccentricity cannot get arbitrary close to unity and are bound by  $e_c = 1 - a_{\text{Neptune}}/a$ , with  $e_c \approx 0.98$ .

The longitude of the ascending nodes show two features. The first is a narrow distribution for the majority of the test particles that follows the precession induced by Planet Nine. Planet Nine’s orbit dominates the dynamical evolution of TAUS. The second is a wider distribution of the minority of the particles as a result of the resonant interaction with Planet Nine, as illustrated in Figure A1.

The argument of periapsis has a wide distribution around  $\sim 200^\circ$ . The inclination distribution is also wide due to strong secular and resonance interactions with Planet Nine. In the TAUS, there are prograde and retrograde orbits. This wide distribution of inclinations give TAUS its spheroidal shape.

### 3.4 Inclined disk

The inclined disk is relatively flat and has an inclination with a mean value  $\langle i \rangle \approx 18.4^\circ$  with respect to the ecliptic. It is located in a region between the TAUS and the ecliptic disk, namely  $1500\text{AU} \lesssim a \lesssim 3000\text{AU}$ . The secular interaction with Planet Nine torques the disk and aligns it towards the orbital plane of Planet Nine (Mouillet et al. 1997). The alignment timescale is of the order of  $\sim$  Gyr, as evident in Figure 1. Figure A2 in the appendix presents the orbital distribution of the test particles that are bounded between  $1500\text{AU} \lesssim a \lesssim 3000\text{AU}$ . The inclined disk has a preferred orientation in space;

the argument of periapsis is clustered around a value of zero (see Figure A2) and the longitude of the ascending node is peaked around  $\sim 100^\circ$ .

### 3.5 Outer disk

The outer disk includes test particles that did not interact with Planet Nine at  $a > 3000\text{AU}$ . The particles show no sign of a change in their initial orbital elements distribution. In other words, the eccentricity, inclination, argument of periapsis and longitude of the ascending nodes distributions, are the same as the initial distributions, as shown in the appendix at Figure A3.

### 3.6 Comparison to a stellar encounter

Next, we compare the signature of the Planet Nine - disk interaction with the perturbation from a close fly-by of a star. We focus on plausible stellar encounters in the local stellar density in the field,  $n_* = 0.1\text{pc}^{-3}$  and a velocity dispersion of stars of  $\sigma_* = 40\text{kms}^{-1}$  (Binney & Tremaine 2008) with a perturber mass of  $m_p \approx 0.5m_\odot$ . We note that in the early star cluster phase that lasts about 100Myr, the conditions could have been completely different with three orders of magnitude higher density  $n_* \approx 100\text{pc}^{-3}$  and a much smaller velocity dispersion of  $\sigma_* = 1\text{kms}^{-1}$  (Li & Adams 2016). We focus just on the stellar encounter in the field because the solar system



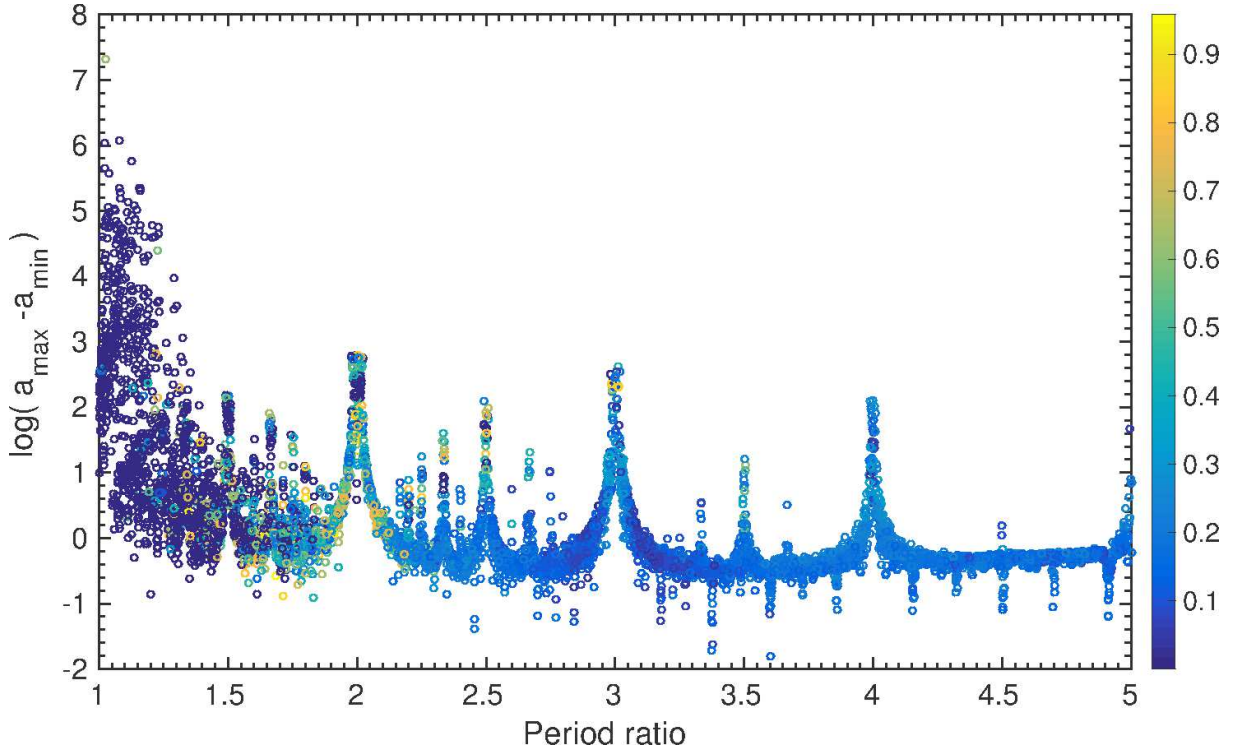


**Figure 5.** A measure of the maximal change in sma as a function of period ratio. The eccentricity is colour coded.

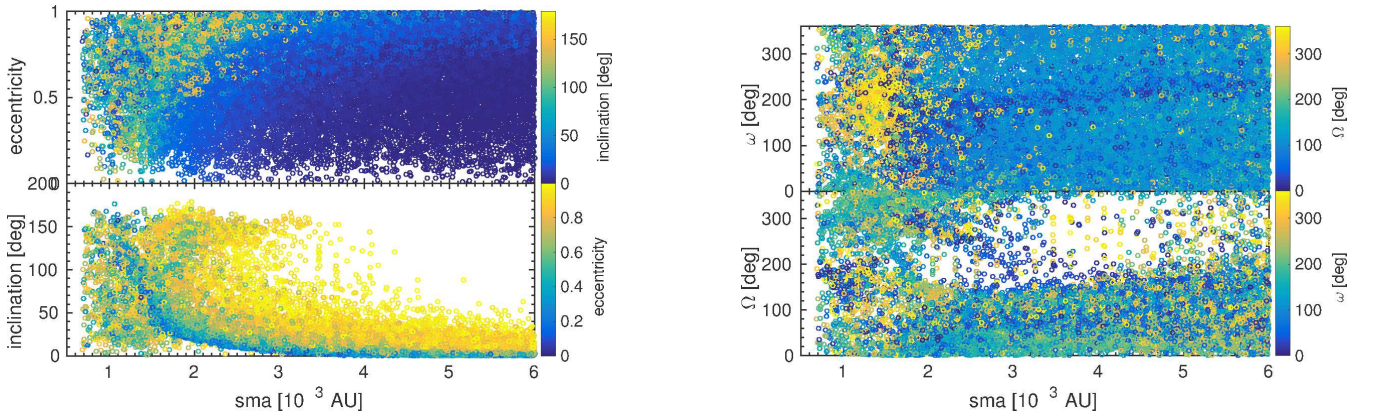


**Figure 6.** **Left panel:** the final state of eccentricities and inclinations as a function of period ratio for scenario (b). **Right panel:** the final distribution of the arguments of pericentre and the longitude of the ascending nodes.

planets were still migrating during the early cluster phase according to popular Nice model (Levison et al. 2008).

The time between stellar encounters,  $t_{\text{enc}}$ , is the inverse of the rate, which in turn proportional to the stellar density,  $n_*$ , the geometrical cross section,  $\sigma_{\text{cross}} = \pi b^2$ , where  $b$  is the impact parameter, and the relative speed at infinity,  $v$

$$\Gamma = n_* \sigma_{\text{cross}} v = n_* \pi b^2 v. \quad (5)$$

Gravitational focusing add a correction to the effective impact parameter

$$b_{\text{focus}}^2 = b^2 \left[ 1 + \left( \frac{v_{\text{esc}}}{v} \right)^2 \right], \quad (6)$$

where  $v_{\text{esc}}$  is the escape velocity at distance  $b$ . For  $b = 1000\text{AU}$ ,  $v_{\text{esc}} \approx 1.3\text{kms}^{-1}$ , yielding negligible gravitational focusing.

Next we calculate  $t_{\text{enc}} = 1/\Gamma$ . For the relevant impact parameter of  $b \approx 1000\text{AU}$  (Hills 1981), the time between encounters is  $t_{\text{enc}} \sim 3.3\text{Gyr}$ , namely roughly once during the lifetime of the solar system.

We simulate such an encounter using MERCURY6 (Chambers 1999) with the Sun and the four giant planets contribution through  $J_2$ . The disk around the Sun is modeled by 1000 massless particles in the same way described in section 2. Additionally, we modeled the stellar encounter to be with  $m_p = 0.5m_{\odot}$  as a hyperbolic trajectory with periastris distance of  $q_p = 1000\text{AU}$ , orbital inclination  $i_p = 90^\circ$ , and an argument of periastris,  $\omega_p = 60^\circ$ . We gave the perturbing star the trajectory that corresponds to  $v_{\infty} = 40\text{kms}^{-1}$  and integrated the system for 1Myr, the orbital properties and the disk morphology are stable after the stellar encounter without any other strong dynamical interactions. Figure 9 shows our simulation

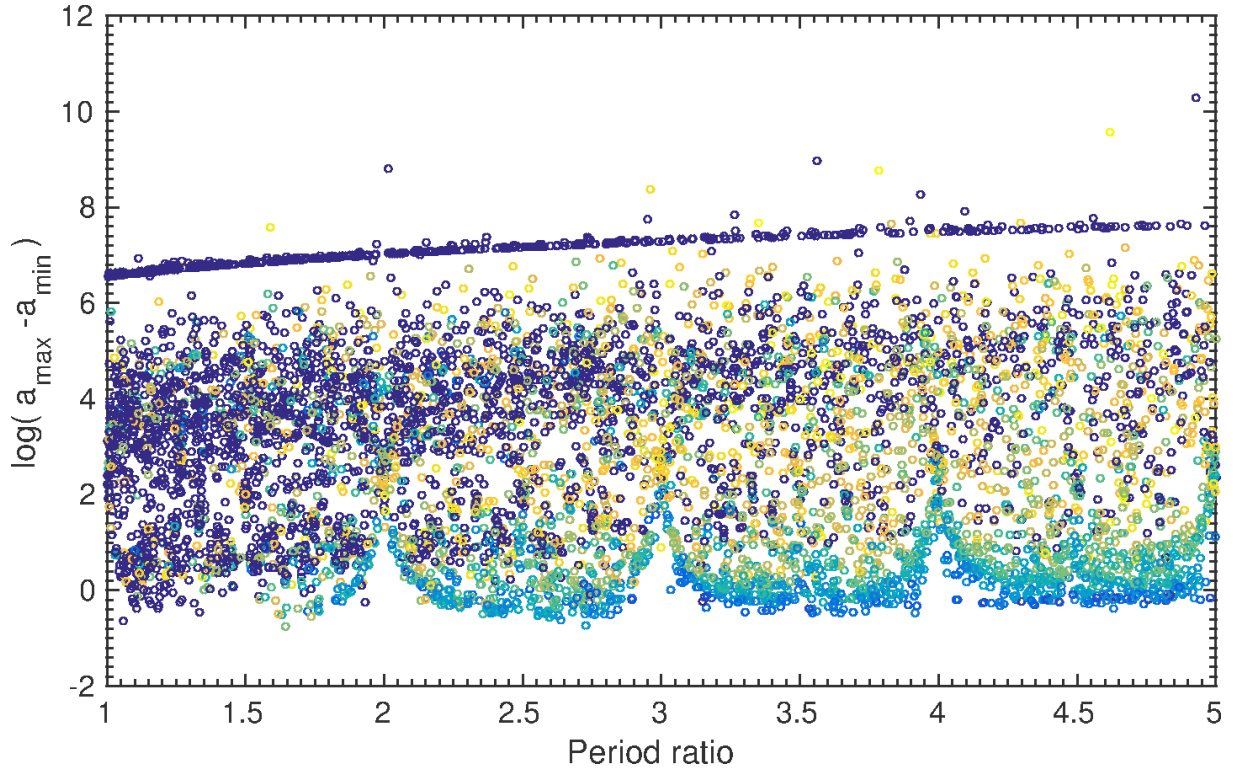


**Figure 7.** A measure of the maximal change in sma as a function of period ratio. The eccentricity is colour coded.

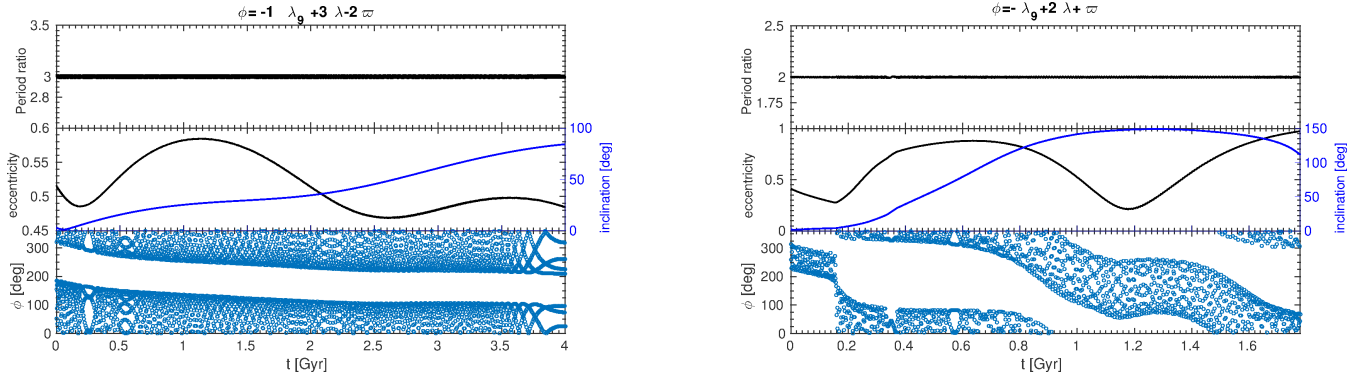


**Figure 8.** **Left panel:** The evolution of single test particle. The particle is in a 3 : 1 MMRs with the resonance angle of  $\phi = -\lambda_9 + 3\lambda - 2\varpi$ . The top panel is the period ratio as a function of time. The middle panel in the eccentricity evolution (black left axis) and the inclination evolution (blue right axis). The bottom panel is the evolution of the resonance angle  $\phi$ . **Right panel:** The evolution of an ejected particle at 2 : 1 MMR with  $\phi = -\lambda_9 + 2\lambda - \varpi$ .

results. Due to the high relative velocity the interaction is extremely weak. The final snapshot from an edge-on projection reveals the main qualitative difference from the Planet Nine scenario. The lack of spheroidal structure is clear visible.

### 3.7 Ejected particles

During our simulation, several particles are dynamically unstable and reach sufficiently high eccentricities  $e > e_c$  to be removed from our simulation. In Figure 10 we present the lost fraction of particles in two representations. First, we show all 32,000 particles and the corresponding loss rate, i.e. the time derivative of the lost fraction. Second, we show the fraction of all particles that initially

have  $a > 1050\text{AU}$  as a function of time and the rate of these events per year.

Figure 11 presents the evolution of two particles that were removed from the system due to their high eccentricity. These particles were ejected at different times from the simulation and become long period comets. These objects originate from the TAUS, and represent a new population of comets. The sma of the removed particles is  $a \sim 1000\text{AU}$  and  $700\text{AU}$ , respectively.

From our simulation we can infer the production rate of comets enter the inner solar system. We present the distribution of orbital parameters for all particles ejected from the simulation in Figure 12. The argument of periapsis is clustered around two values:  $\sim 40^\circ$  and  $\sim 180^\circ$ , while the longitude of the ascending node is clustered around  $\sim 0$  and  $\sim 150^\circ$ . The inclination is also clustered around two

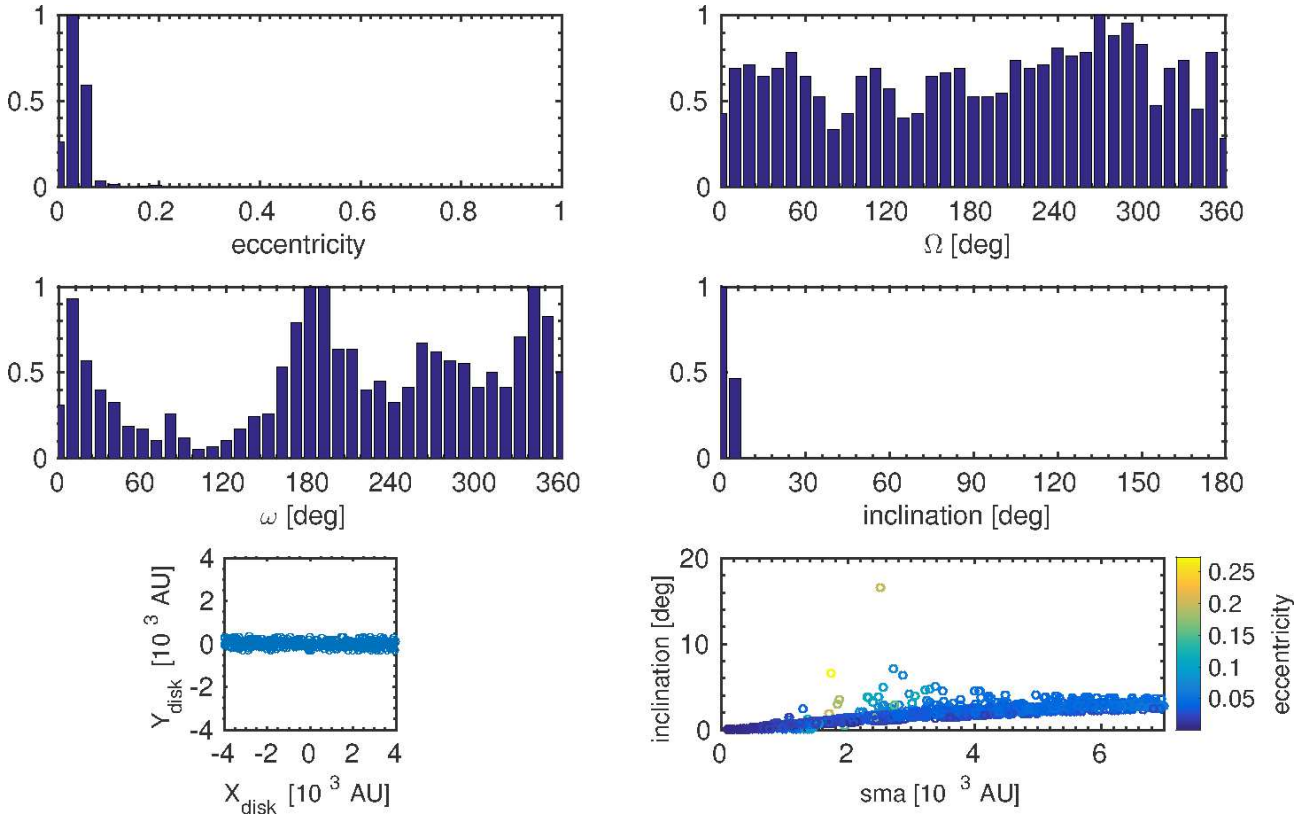


**Figure 9.** **Upper left:** The eccentricity distribution is sharply around  $\sim 0.05$ . **Upper right:** The longitude of ascending nodes,  $\Omega$ , has a near uniform distribution. **Middle left:** The argument of periapsis,  $\omega$ , has a wide distribution. **Middle right:** The inclination distribution. The disk remains flat. **Bottom left:** Final snapshot of the disk after a stellar encounter. The disk is on the X-Z plane. **Bottom right:** The inclination as a function of sma (the eccentricity colour coded) shows a weak dependence on sma.

values:  $\sim 40^\circ$  and  $\sim 140^\circ$ . Figure A5 presents the same as figure 12 for scenario (b). We find that the rate of the ejected particles in scenario (b) is higher by an order of magnitude compared with scenario (a).

## 4 IMPLICATIONS AND DISCUSSION

Assuming that Planet Nine captured in the early stages of the solar system lifetime, it must have interacted with the disk of planetesimal around it. We chose the simplest structure of a debris disk that is initially flat and circular. Our initial conditions are conservative in the sense that disk, that is more inclined or eccentric would have a lower specific angular momentum and therefore would tend to be more influenced by Planet Nine. We have found that a spheroidal structure (TAUS) is created around the Sun at  $\sim 1200\text{AU}$  and is surrounded by an inclined disk beyond  $\sim 1500\text{AU}$ .

### 4.1 New structure in the solar-system

The TAUS is a spheroidal structure. It does not represent a perfect sphere because the particles' longitude of the ascending nodes is not uniformly distributed. This implies that some parts of the sphere are populated more than others. The number of particles in the TAUS is not well constrained, as it depends on the initial conditions, number of particles in the disk and their surface density distribution. Scenario (a) and (b) differ in the size of the TAUS; in scenario (a) TAUS end at  $\sim 1500\text{AU}$  while in scenario (b) at  $\sim 3000\text{AU}$ . We

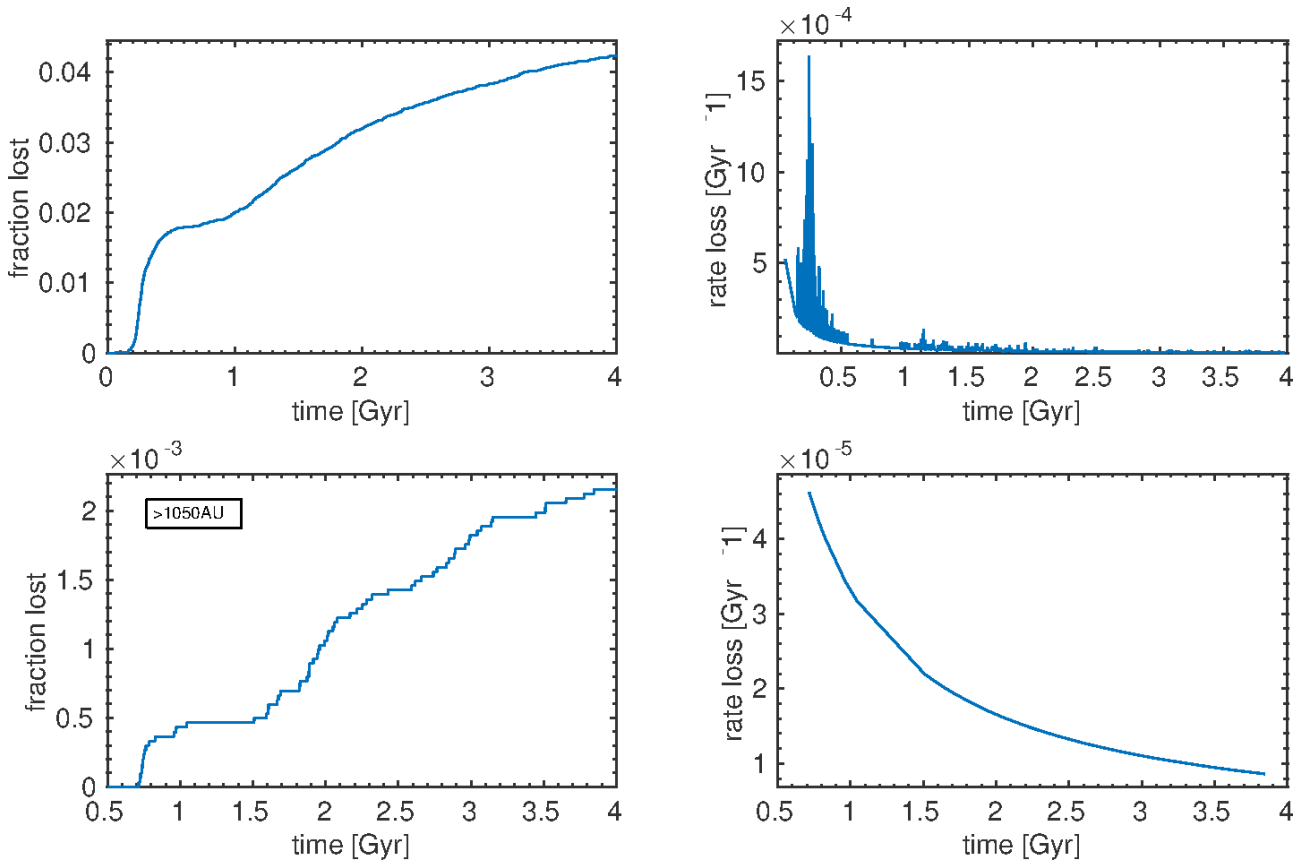
assumed the power law index of the density distribution be  $\gamma = -1$ . Unlike the Oort cloud at  $\sim 10^5\text{AU}$  or even the Hills cloud at  $\sim 10^4\text{AU}$  the TAUS is relatively close and perhaps could be detected by a dedicated infrared survey.

Figure 10 implies that in the early stage of the solar system evolution, around 300Myr after formation, there was a spike in the rate of ejected objects from the disk into the inner solar systems, by up to two orders of magnitude relative to the current rate. This implies that there was an epoch during which a large number of objects from the region of  $\sim 1000\text{AU}$  crossed the orbits of the inner planets, similarly to the ‘‘heavy bombardment’’ epoch described in the Nice model (Levison et al. 2008).

### 4.2 New origin of comets

Some TAUS objects are excited to high eccentricities due to resonance and secular interaction with Planet Nine (see section 3.7). These objects enter the solar system with eccentricities close to unity and therefore can be considered as comet candidates. Due to the specific orientation of the TAUS, we expect the comets to originate from  $1100\text{AU} \lesssim a_{\text{comet}} \lesssim 1500\text{AU}(3000\text{AU})$ , and have the distribution of the specific argument of periapsis, longitude of the ascending node and inclination shown in Figures 12 and A4. This is a prediction of our model that can be tested observationally. For a total number of objects in the TAUS,  $N$ , one can estimate the rate





**Figure 10.** **Upper left:** Loss fraction from the entire population of particles. During the integration time  $\sim 2\%$  of the particles were removed after entering the inner solar system. **Upper right:** The rate of ejection as a function of time. This panel is the time derivative of the left panel. **Bottom left:** Loss fraction from the overall particles with initial sma greater than 1050AU. **Bottom right:** The rate of ejection as a function of time. Both plots shows a high loss rate at  $\sim 300$  Myr which implies large number of objects interacting with Planet Nine in this era.

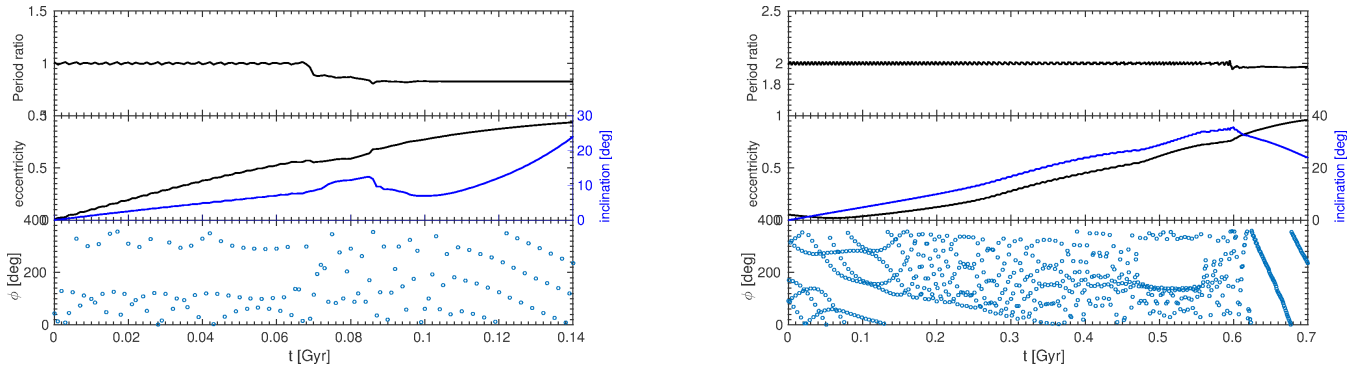


**Figure 11.** The same as figure 8. **Left panel:** The particle is in a 1 : 1 MMRs with Planet Nine. **Right panel:** The evolution of an ejected particle at 2 : 1 MMR with  $\phi = -\lambda_9 + 2\lambda$ .

of these events per year, as

$$\Gamma_{\text{comet}} \sim 10^{-2} - 10^{-1} \text{yr}^{-1} \left( \frac{N}{10^{12}} \right). \quad (7)$$

The Large Synoptic Survey Telescope (LSST) will survey 20,000 square degrees of the sky about 2,000 times over 10 years (LSST Science Collaboration et al. 2009). This survey is expected to discover 10, 000 new comets and potentially shed light on the size distribution of long period comets, which is currently unknown. The

Starshot Breakthrough Initiatives could also explore the solar system (<http://breakthroughinitiatives.org/Concept/3/>).

The gravitational interaction of the comet candidates with the solar systems planets was not explored here. An extensive study on this interaction and its observational signatures will be studied elsewhere.



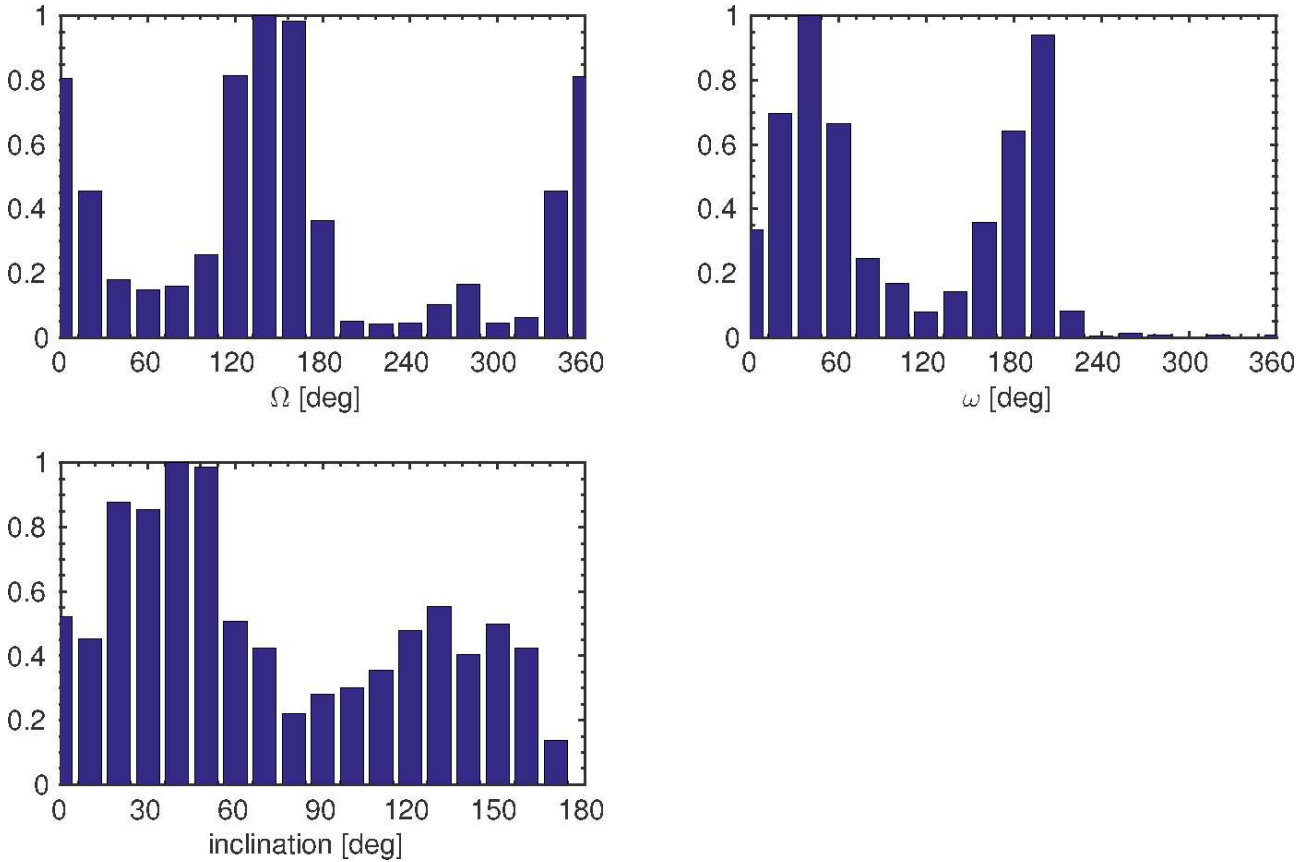


**Figure 12.** Orbital parameter distributions of the removed particles from the simulation. The argument of periapsis has two sharp peaks around:  $\sim 40^\circ$  and  $\sim 140^\circ$ . The inclination distribution is wide with two wide bumps around:  $\sim 20^\circ - 50^\circ$  and  $\sim 120^\circ - 150^\circ$ . The longitude of ascending nodes has two sharp bumps around:  $\sim 0$  and  $\sim 140^\circ$ . All distribution are normalized a maximum value of unity.

## 5 SUMMARY

We calculated the dynamical imprint of Planet Nine on the outer solar system, assuming a flat circular initial debris disk out to a distance of 7000AU. We showed that orbits with  $a < 3000$  AU interacted with Planet Nine over the lifetime of the solar system.

Our main conclusions are as follows:

- A spheroidal structure, TAUS, forms at  $\sim 1200$  AU due to MMRs with Planet Nine.
- TAUS is not uniformly distributed.
- The interaction of Planet Nine with the disk produces a qualitatively different morphology than a fly-by interaction with a passing star.
- Objects from TAUS that are excited to high eccentricities could become comets.

These predictions can be tested observationally with future surveys such as LSST or the Starshot Breakthrough Initiative.

## ACKNOWLEDGEMENTS

We thank Matt Holman and Hagai B. Perets for helpful comments on the manuscript. E.M. thanks Harvard’s Institute for Theory and Computation (ITC) for its kind hospitality during August 2016, when this paper was initiated. E.M also acknowledges the European union career integration grant “GRAND,” and the Israel science foundation excellence centre I-CORE grant 1829/12.

## REFERENCES

- Andrews S. M., Wilner D. J., Hughes A. M., Qi C., Dullemond C. P., 2010, *ApJ*, **723**, 1241
- Bailey E., Batygin K., Brown M. E., 2016, *AJ*, **152**, 126
- Batygin K., Brown M. E., 2016, *AJ*, **151**, 22
- Binney J., Tremaine S., 2008, *Galactic Dynamics: Second Edition*. Princeton University Press
- Brown M. E., Batygin K., 2016, *ApJ*, **824**, L23
- Chambers J. E., 1999, *MNRAS*, **304**, 793
- Duncan M., Quinn T., Tremaine S., 1987, *AJ*, **94**, 1330
- Fienga A., Laskar J., Manche H., Gastineau M., 2016, *A&A*, **587**, L8
- Gomes R., Deienno R., Morbidelli A., 2017, *AJ*, **153**, 27
- Hills J. G., 1981, *AJ*, **86**, 1730
- Holman M. J., Payne M. J., 2016, preprint, ([arXiv:1604.03180](https://arxiv.org/abs/1604.03180))
- Kalas P., Larwood J., Smith B. A., Schultz A., 2000, *ApJ*, **530**, L133
- LSST Science Collaboration et al., 2009, preprint, ([arXiv:0912.0201](https://arxiv.org/abs/0912.0201))
- Lai D., 2016, *AJ*, **152**, 215
- Larwood J., Kalas P., 2000, *ArXiv Astrophysics e-prints*,
- Lawler S. M., Shankman C., Kaib N., Bannister M. T., Gladman B., Kavelaars J. J., 2016, preprint, ([arXiv:1605.06575](https://arxiv.org/abs/1605.06575))
- Lee E. J., Chiang E., 2016, *ApJ*, **827**, 125
- Levison H. F., Morbidelli A., Van Laerhoven C., Gomes R., Tsiganis K., 2008, *Icarus*, **196**, 258
- Li G., Adams F. C., 2016, *ApJ*, **823**, L3
- Marsden B. G., Sekanina Z., Everhart E., 1978, *AJ*, **83**, 64
- Morbidelli A., Thomas F., Moons M., 1995, *Icarus*, **118**, 322
- Mouillet D., Larwood J. D., Papaloizou J. C. B., Lagrange A. M., 1997, *MNRAS*, **292**, 896
- Murray C. D., Dermott S. F., 1999, *Solar system dynamics*

Oort J. H., 1950, *Bull. Astron. Inst. Netherlands*, **11**, 91  
Perets H. B., Kouwenhoven M. B. N., 2012, *ApJ*, **750**, 83  
Trujillo C. A., Sheppard S. S., 2014, *Nature*, **507**, 471  
Veras D., Evans N. W., 2013, *MNRAS*, **430**, 403

## **APPENDIX A: DISK DISTRIBUTIONS**

In the appendix we present the test particles orbital properties for the three different regimes: (i) TAUS ;(ii) an inclined disk and (iii) a warped disk relative to the ecliptic plane. Moreover we present the properties of the ejected particles from scenario (b).

This paper has been typeset from a  $\text{\TeX/L\AA\TeX}$  file prepared by the author.

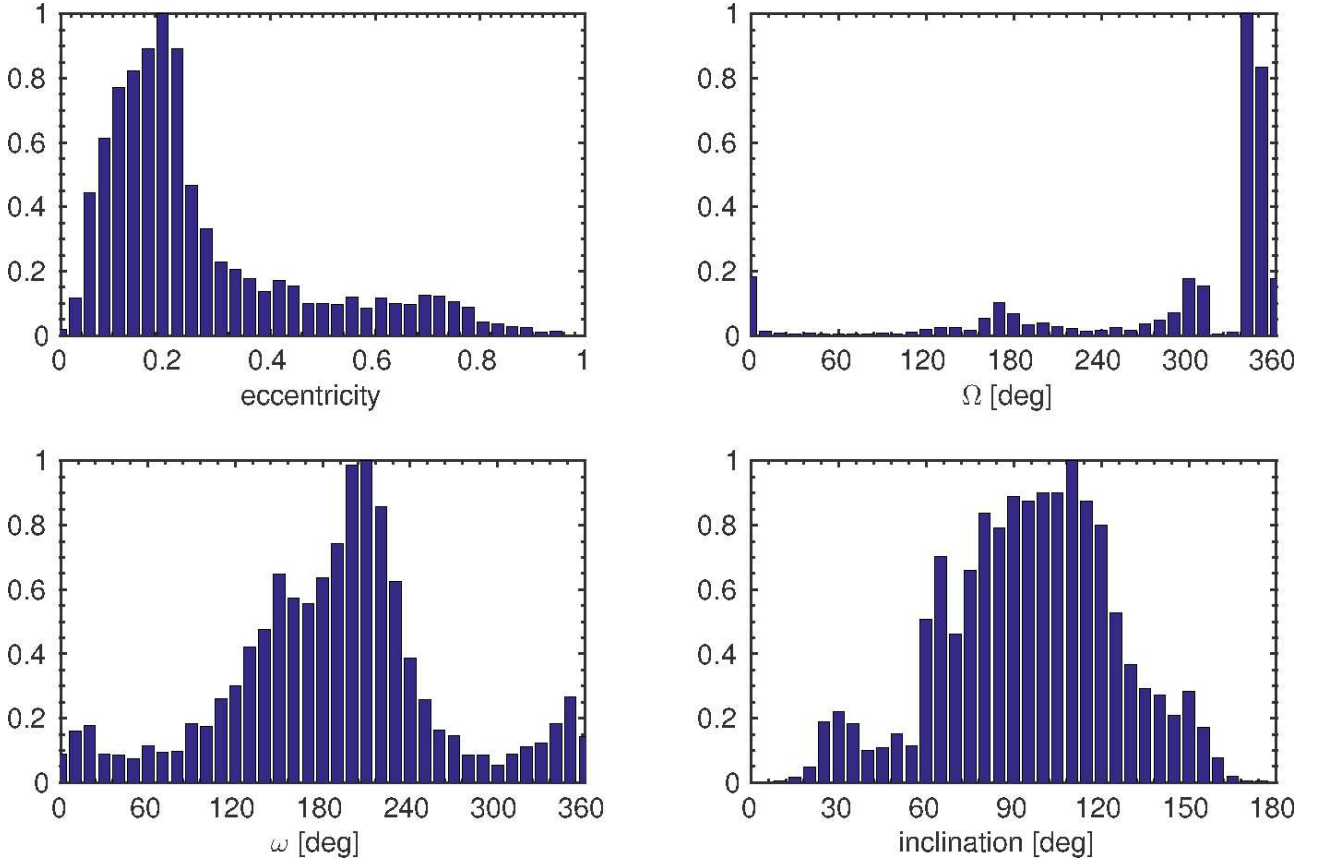


**Figure A1.** Final distributions of the eccentricity, longitude of ascending node and the argument of the periastron for TAUS. **Upper left:** The eccentricity distribution is concentrated around  $e \approx 0.2$ , with a tail of highly eccentric orbits (which are stable on a 4 Gyr timescale). **Upper right:** The longitude of ascending nodes show two characteristics: a narrow distribution around  $\Omega \approx 350^\circ$  and a wide spread tail. **Bottom left:** The argument of periastron,  $\omega$ , have a wider distribution around  $\sim 200^\circ$ . **Bottom right:** The inclination distribution spans the range between  $\sim 30^\circ$  and  $\sim 160^\circ$ , which gives the TAUS is spheroidal shape. All distributions are normalized to the maximal value of unity.

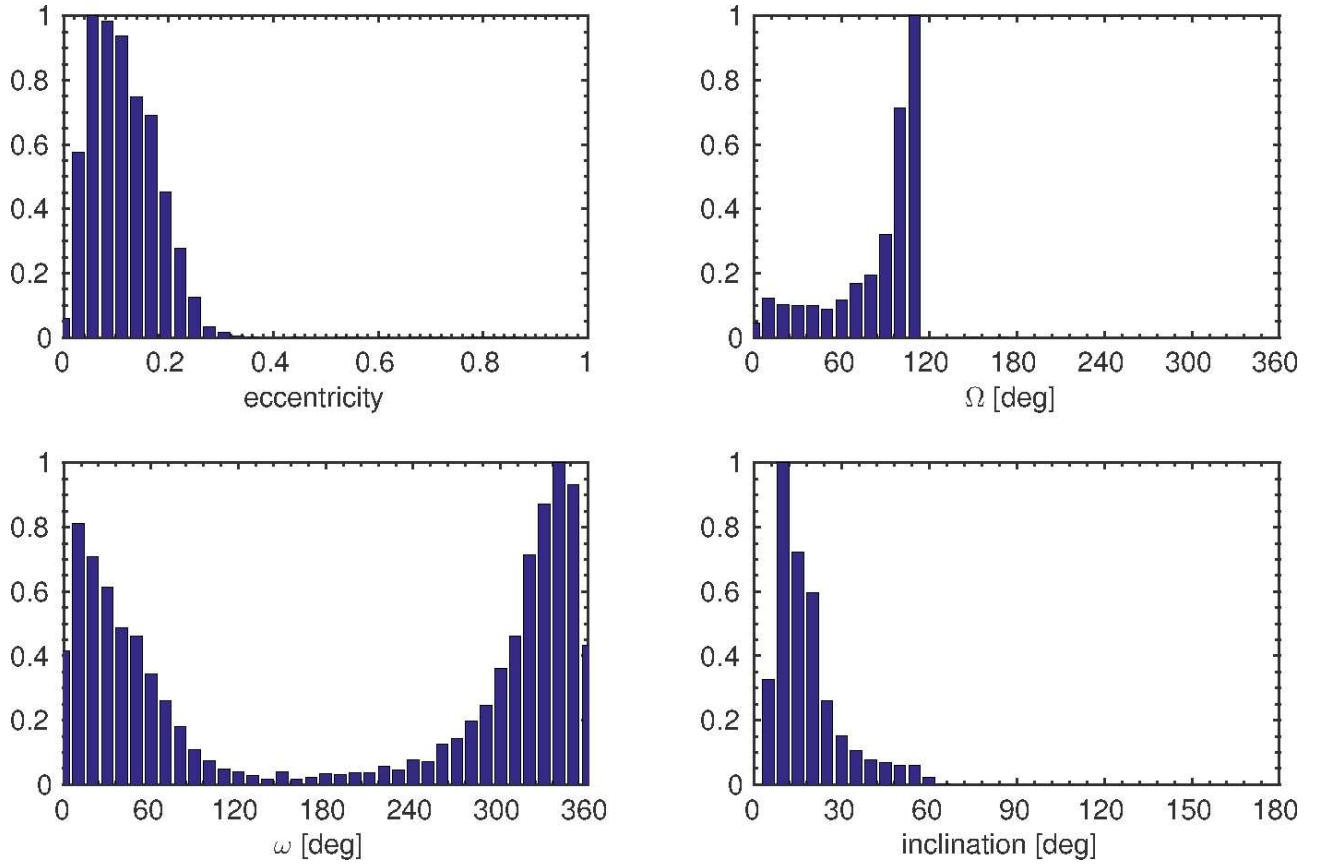


**Figure A2.** Final distributions of the eccentricity, longitude of ascending node and the argument of periastris for the inclined disk. **Upper left:** The eccentricity distribution is concentrated around  $e \approx 0.1$ . **Upper right:** The longitude of the ascending nodes shows a sharp cutoff at  $\sim 110^\circ$ . **Bottom left:** The argument of the periastris is clustered around  $\sim 0$ . **Bottom right:** The inclination distribution is narrow with mean inclination of  $18.4^\circ$ .



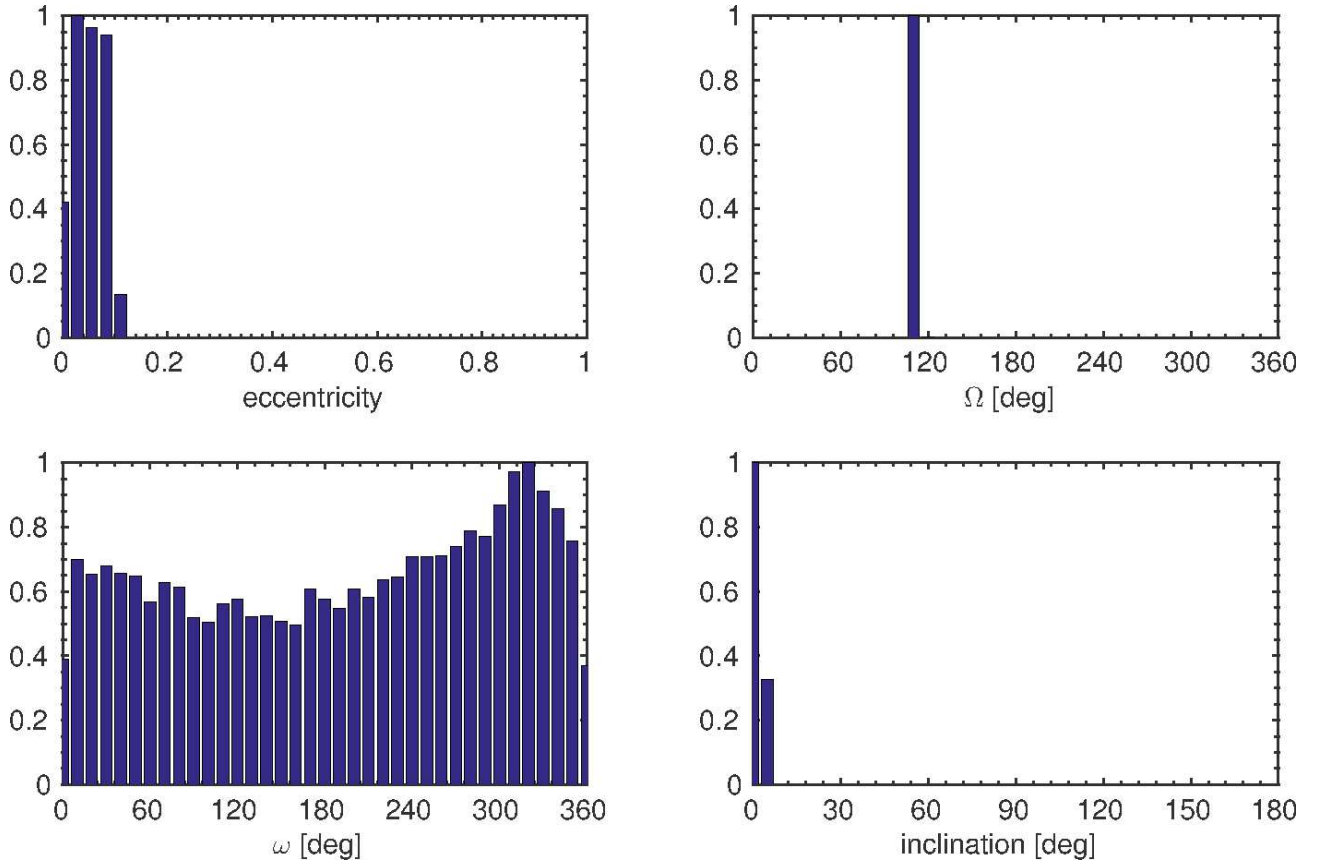


**Figure A3.** Final distribution of the eccentricity, longitude of ascending nodes and the argument of periapsis for the outer disk. The distributions appear to follow the initial distributions. This part of the disk did not have sufficient time to interact with Planet Nine during the lifetime of the solar system.

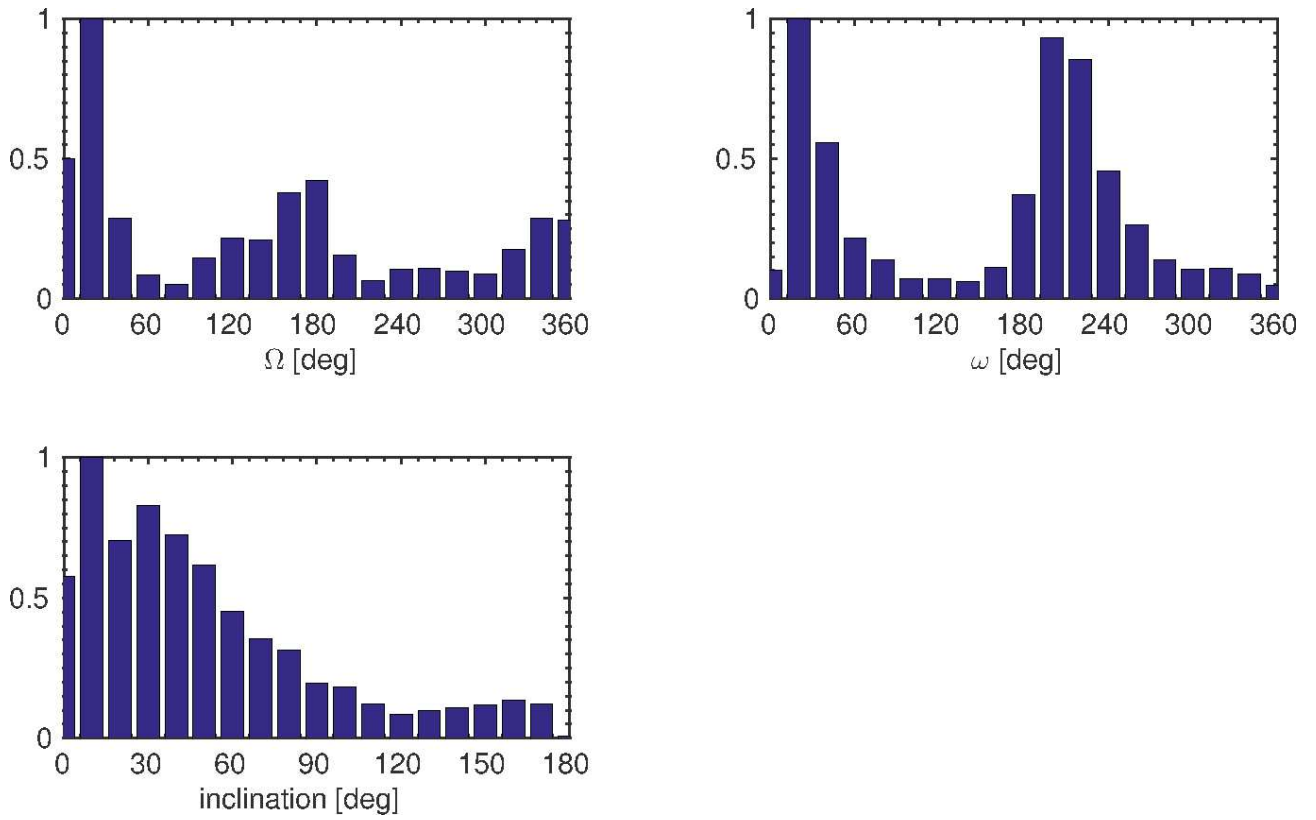


**Figure A4.** Orbital parameter distributions of the removed particles from the simulation from scenario (b), i.e. Sun grazing comets candidates. The argument of periaapsis has two sharp peaks around:  $\sim 30^\circ$  and  $\sim 200^\circ$ . The inclination distribution is wide. The longitude of ascending nodes has two sharp bumps around:  $\sim 20$  and  $\sim 180^\circ$ . All distribution are normalized a maximum value of unity.

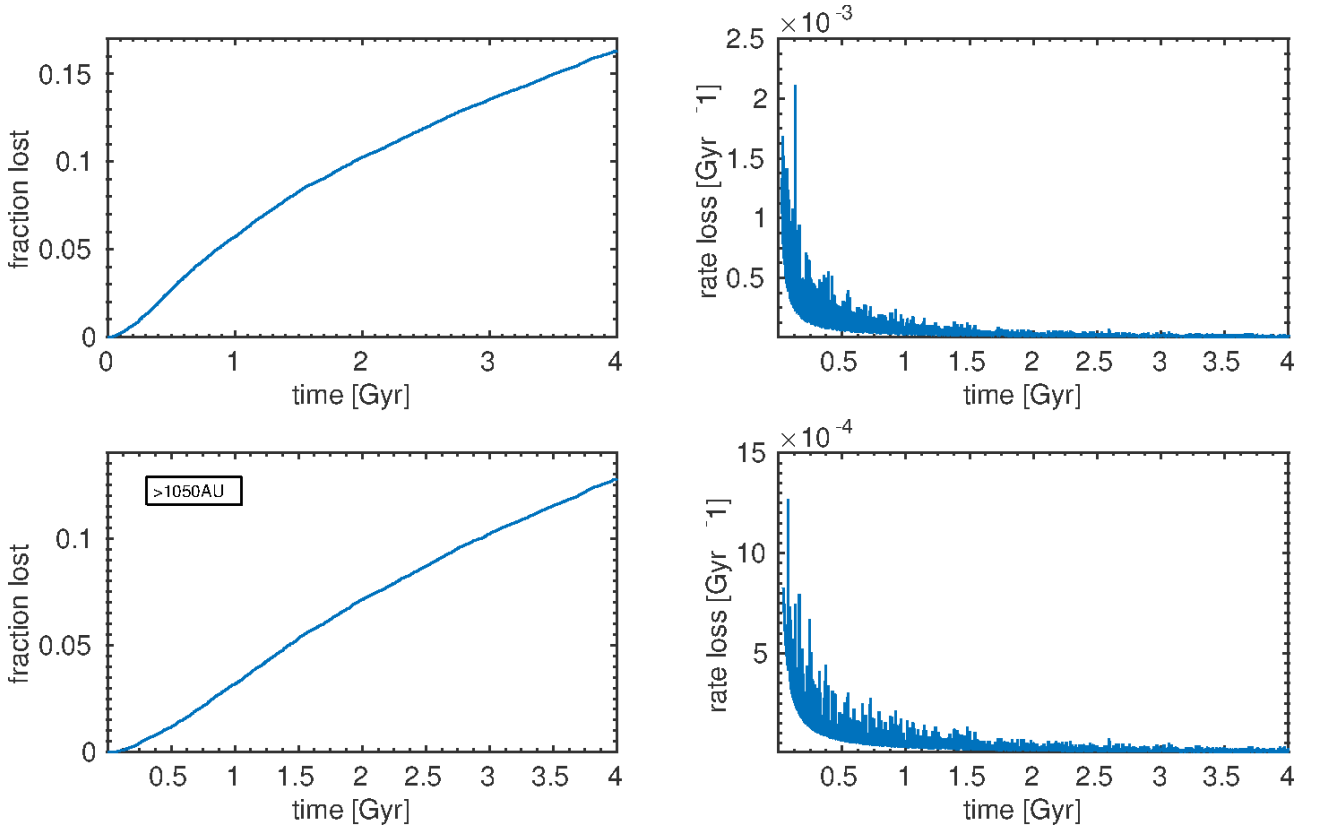


**Figure A5. Upper left:** Loss fraction from the entire population of particles of scenario (b). During the integration time  $\sim 2\%$  of the particles were removed after entering the inner solar system. **Upper right:** The rate of ejection as a function of time. This panel is the time derivative of the left panel. **Bottom left:** Loss fraction from the overall particles with initial  $sma$  greater than 1050AU. **Bottom right:** The rate of ejection as a function of time. We note that in this scenario the fraction loss and the loss rate is higher by an order of magnitude than scenario (a).